

Switchable vortex beam polarization state terahertz multi-layer metasurface

Min Zhong(仲敏), Jiu-Sheng Li(李九生)

Citation: Chin. Phys. B, 2022, 31 (**11**): 114201. DOI: 10.1088/1674-1056/ac7cd2

What follows is a list of articles you may be interested in

Switchable vortex beam polarization state terahertz multi-layer metasurface

Min Zhong(仲敏), Jiu-Sheng Li(李九生)
Chin. Phys. B, 2022, 31 (**11**): 114201. DOI: 10.1088/1674-1056/ac7cd2

Circular dichroism spectra of α-lactose molecular measured by terahertz time-domain spectroscopy

Chun Wang(王春), Bo Wang(王博), Gaoshuai Wei(魏高帅), Jianing Chen(陈佳宁), and Li Wang(汪力)
Chin. Phys. B, 2022, 31 (**10**): 104201. DOI: 10.1088/1674-1056/ac6edb

Multi-function terahertz wave manipulation utilizing Fourier convolution operation metasurface

Min Zhong(仲敏) and Jiu-Sheng Li(李九生)
Chin. Phys. B, 2022, 31 (**5**): 054207. DOI: 10.1088/1674-1056/ac46c0

Creation of multi-frequency terahertz waves by optimized cascaded difference frequency generation

Zhong-Yang Li(李忠洋), Jia Zhao(赵佳), Sheng Yuan(袁胜), Bin-Zhe Jiao(焦彬哲), Pi-Bin Bing(邴丕彬), Hong-Tao Zhang(张红涛), Zhi-Liang Chen(陈治良), Lian Tan(谭联), and Jian-Quan Yao(姚建铨)
Chin. Phys. B, 2022, 31 (**4**): 044205. DOI: 10.1088/1674-1056/ac29b4

High-sensitive terahertz detection by parametric up-conversion using nanosecond pulsed laser

Yuye Wang(王与烨), Gang Nie(聂港), Changhao Hu(胡常灏), Kai Chen(陈锴), Chao Yan(闫超), Bin Wu(吴斌), Junfeng Zhu(朱军峰), Degang Xu(徐德刚), and Jianquan Yao(姚建铨)
Chin. Phys. B, 2022, 31 (**2**): 024204. DOI: 10.1088/1674-1056/ac2d20

Switchable vortex beam polarization state terahertz multi-layer metasurface

Min Zhong(仲敏) and Jiu-Sheng Li(李九生)†

Center for THz Research, China Jiliang University, Hangzhou 310018, *China*

(Received 5 June 2022; revised manuscript received 27 June 2022; accepted manuscript online 29 June 2022)

We propose a switchable vortex beam polarization state terahertz multi-layer metasurface, which consists of three-layer elliptical metal crosses, four-layer dielectrics, and two-layer hollow metal circles, which are alternately superimposed. Under the normal incidence of left-handed circularly polarized (LCP) wave and the right-handed circularly polarized (RCP) waves, the proposed structure realizes three independent control functions, *i.e.*, focused and vortex beam, vortex beam with different topological charges, and polarization states switching, and azimuth switching of two vortex beams with different polarization states. The results show that the proposed metasurface provides a new idea for investigating the multifunctional terahertz wave modulation devices.

Keywords: terahertz wave, switchable vortex beam, polarization states, flexible manipulation

PACS: 42.25.Ja, 74.25.Uv, 07.05.Tp **DOI:** 10.1088/1674-1056/ac7cd2

1. Introduction

Metasurface can flexibly manipulate the phase, amplitude, polarization, frequency, and wavefront propagation of electromagnetic wave and possesses many applications in holographic projection,[1,2] focusing,[3–5] photon spin Hall effect,[6–9] Airy beam,[10,11] spectrum,[12] *etc*. Recently, vortex generators based on metasurface orbital angular momentum (OAM) have attracted much attention.[13–15] For example, in 2019, Liu *et al*.[16] proposed a multifunctional metasurface vortex beam generator to realize vortex beams with reconfigurable polarization states. In 2020, Jiang *et al*.[17] designed a plasma metasurface vortex beam generator to generate near-field dual-channel vortex beam and far-field dual-channel vortex beam. In 2021, Zheng *et al*.[18] designed a metasurface by changing the opening angle and direction angle of the square split ring to obtain about 80% high-purity mode vortex beams. More recently, some research teams have drawn their attention towards Pancharatnam–Berry (PB) metasurface vortex generator.[19–21] In 2021, Gao *et al*.[22] employed a four-layer metallic PB phase metasurface and a three-layer dielectric PB phase metasurface to obtain a vortex beam with a transmission efficiency of about 79%. Wang *et al*.[23] utilized a flexible bilayer PB phase metasurface to generate vortex beams for circularly polarized waves incidence. In 2022, Xiang *et al*.[24] proposed a TiO_2 elliptical cylinder all-dielectric PB phase metasurface for generating annular focused optical vortices. However, PB-phase metasurfaces can only realize spin-locked OAM beams or OAM beams with specific helicity. This effect is the inherent characteristics of geometric phase metasurfaces, which limit the device application. Furthermore, independent control of OAM with two different helicities remains a problem, especially in the terahertz band, which is still a challenge.

In this work, we combine propagation phase and geometric phase to design a switchable vortex beam polarization state multi-layer metasurface in terahertz region. By changing the size parameters and rotation angle of the metal–particle at the same time, the decoupling relationship between the incidence of left-handed circularly polarized (LCP) wave and the incidence of right-handed circularly polarized (RCP) wave is established. Therefore, the two orthogonal circularly polarized waves can generate mutually independent functions. The designed metasurface generates switching between focused beam and vortex beam, switching between vortex beams with different topological charges, azimuth switching between two vortex beams under different circularly polarized waves incident. The designed metasurface has potential applications in terahertz control devices.

2. Device design

Figure 1 shows the schematic diagram of the switchable vortex beam polarization state terahertz multi-layer metasurface, which can exhibit different and independent functions under the incidence of two different circularly polarized waves. This metal particle is composed of three elliptical metal cross layers, four dielectric layers and two hollow metal circle layers. The metallic material is gold with a conductivity of 4.561×10^7 S/m. The thickness of metal layer is 3 μm, and the dielectric layer is polyimide with a thickness of 10 μm. The arm lengths of the elliptical metal cross are marked as a and b, respectively. The radius of the hollow metal circle is $r = 20$ μm, and the period of the metal particle is set to be $p = 130$ μm. We use the commercial CST Microwave Studio to optimize the coding particle under the incidence of LCP wave and RCP wave. Both x axis and y axis are set to be of periodic boundary conditions and z axis is fixed as open space.

†Corresponding author. E-mail: lijsh2008@126.com

© 2022 Chinese Physical Society and IOP Publishing Ltd

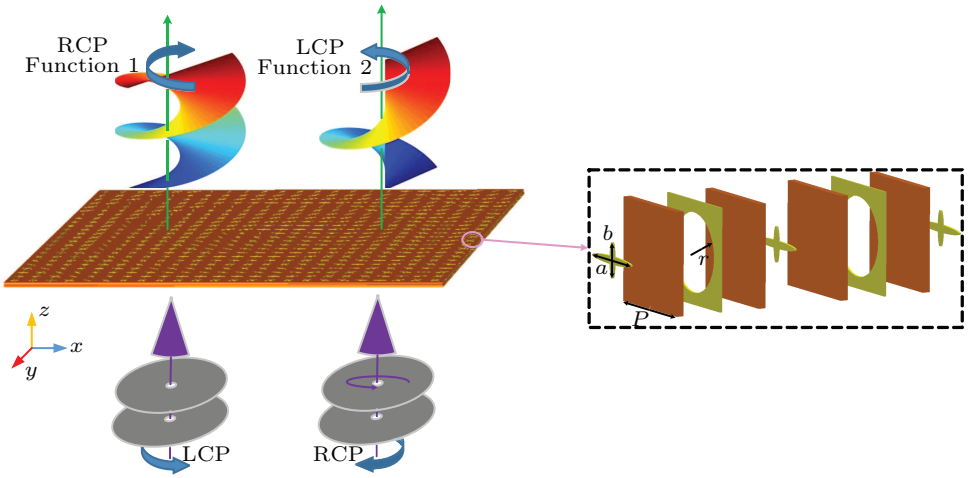


Fig. 1. Schematic diagram of switchable vortex beam polarization state terahertz multi-layer metasurface.

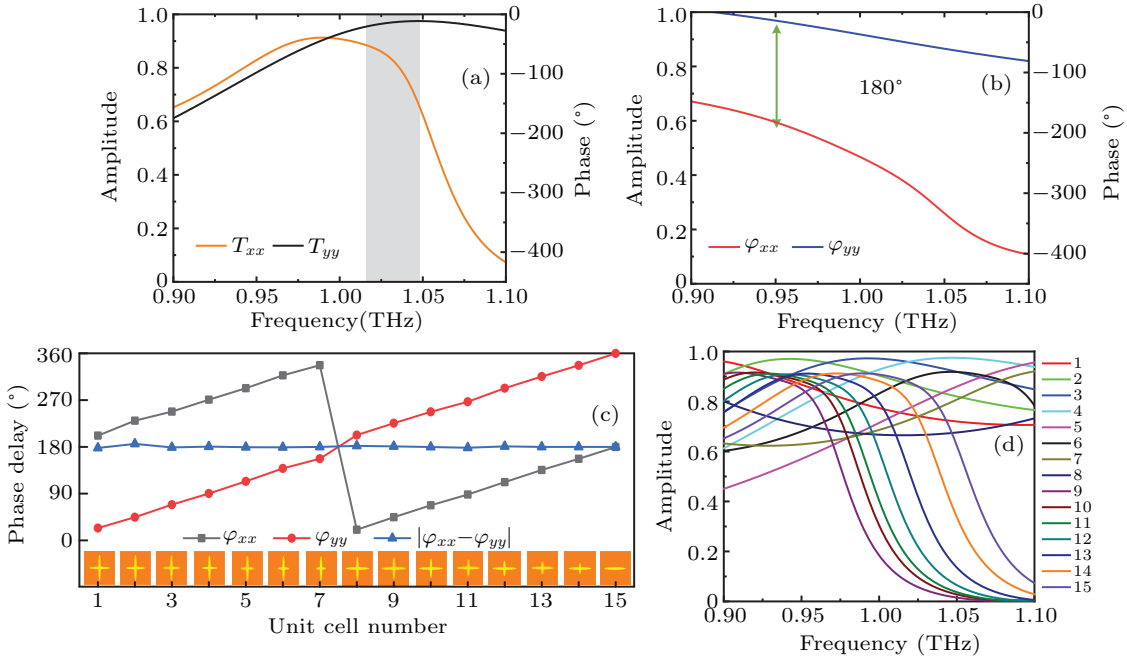


Fig. 2. Under linearly polarized terahertz wave incidence, (a) transmission amplitude and (b) phase of particle, (c) phase and (d) amplitude of 15 metal-particles with different sizes.

Under the incidence of circularly polarized terahertz wave, the relationship matrix between the transmitted field and the incident field can be expressed as

$$\begin{pmatrix} \boldsymbol{E}_{\mathrm{L}}^{\mathrm{t}} \\ \boldsymbol{E}_{\mathrm{R}}^{\mathrm{t}} \end{pmatrix} = \begin{pmatrix} T_{\mathrm{LL}} & T_{\mathrm{LR}} \\ T_{\mathrm{RL}} & T_{\mathrm{RR}} \end{pmatrix} \cdot \begin{pmatrix} \boldsymbol{E}_{\mathrm{L}}^{\mathrm{i}} \\ \boldsymbol{E}_{\mathrm{R}}^{\mathrm{i}} \end{pmatrix}, \tag{1}$$

where T_{LL}, T_{LR}, T_{RL}, and T_{RR} are the transmission coefficients (the first subscript and the second subscript respectively represent the polarization state of transmitted wave and reflected wave). After introducing propagation phase and geometric phase, the relationship matrix can be given by

$$\begin{pmatrix} \boldsymbol{E}_{\mathrm{L}}^{\mathrm{t}} \\ \boldsymbol{E}_{\mathrm{R}}^{\mathrm{t}} \end{pmatrix} = \begin{pmatrix} \eta\, \mathrm{e}^{-\mathrm{i}2\alpha} & \delta \\ \delta & \eta\, \mathrm{e}^{\mathrm{i}2\alpha} \end{pmatrix} \cdot \begin{pmatrix} \boldsymbol{E}_{\mathrm{L}}^{\mathrm{i}} \\ \boldsymbol{E}_{\mathrm{R}}^{\mathrm{i}} \end{pmatrix}, \tag{2}$$

where α is the rotation angle of the unit cell, $\delta = (T_x \mathrm{e}^{\mathrm{i}\varphi x} + T_y \mathrm{e}^{\mathrm{i}\varphi y})/2$, $\eta = (T_x \mathrm{e}^{\mathrm{i}\varphi x} - T_y \mathrm{e}^{\mathrm{i}\varphi y})/2$. T_x, T_y, φ_x, and φ_y represent the transmission amplitude and transmission phase of the x-polarized and y-polarized waves, respectively. When the amplitude of the incident polarized wave is 1, the phase difference is π (*i.e.*, $R_x = R_y = 1$, $\varphi_x - \varphi_y = 180°$), $\delta = (T_x \mathrm{e}^{\mathrm{i}\varphi x} + T_y \mathrm{e}^{\mathrm{i}\varphi y})/2 = 0$, $\eta = (T_x \mathrm{e}^{\mathrm{i}\varphi x} - T_y \mathrm{e}^{\mathrm{i}\varphi y})/2 = (\mathrm{e}^{\mathrm{i}\varphi x} - \mathrm{e}^{\mathrm{i}(\varphi x - 180°)})/2 = \mathrm{e}^{\mathrm{i}\varphi x}$. The transmission matrix can be given by

$$\begin{aligned} \begin{pmatrix} \boldsymbol{E}_{\mathrm{L}}^{\mathrm{t}} \\ \boldsymbol{E}_{\mathrm{R}}^{\mathrm{t}} \end{pmatrix} &= \begin{pmatrix} \mathrm{e}^{\mathrm{i}(\varphi x - 2\alpha)} & 0 \\ 0 & \mathrm{e}^{\mathrm{i}(\varphi x + 2\alpha)} \end{pmatrix} \cdot \begin{pmatrix} \boldsymbol{E}_{\mathrm{L}}^{\mathrm{i}} \\ \boldsymbol{E}_{\mathrm{R}}^{\mathrm{i}} \end{pmatrix} \\ &= \begin{pmatrix} \mathrm{e}^{\mathrm{i}(\varphi x - 2\alpha)} \boldsymbol{E}_{\mathrm{L}}^{\mathrm{i}} \\ \mathrm{e}^{\mathrm{i}(\varphi x + 2\alpha)} \boldsymbol{E}_{\mathrm{R}}^{\mathrm{i}} \end{pmatrix}. \end{aligned} \tag{3}$$

From the above equation, it can be found that the LCP wave and the RCP wave of the transmitted field each acquire an extra phase (*i.e.*, $\varphi_{\mathrm{L}} = \varphi_x - 2\alpha$, $\varphi_{\mathrm{R}} = \varphi_x + 2\alpha$), which can be

expressed as

$$\begin{cases} \alpha = (\varphi_{\mathrm{R}} - \varphi_{\mathrm{L}})/4, \\ \varphi_x = (\varphi_{\mathrm{R}} + \varphi_{\mathrm{L}})/2, \\ \varphi_y = (\varphi_{\mathrm{R}} + \varphi_{\mathrm{L}})/2 - 180^\circ. \end{cases} \tag{4}$$

It can be seen from the above formula that the decoupling of the relationship between the LCP wave and RCP wave can be achieved by adjusting the rotation angle α of the metal-particle, the transmission phase φ_x and φ_y of x- and y-polarized waves.

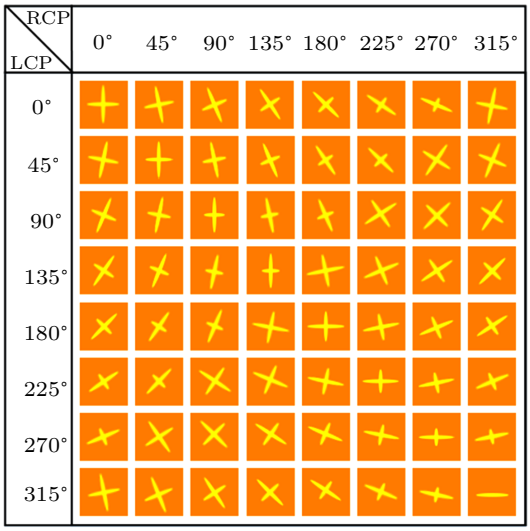


Fig. 3. The 64 kinds of metal-particles.

Figures 2(a) and 2(b) display the transmission amplitude and phase of metal-particle under the incidence of linearly polarized terahertz waves. At a frequency of 0.97 THz, the metal-particle has a high transmission amplitude, and the phase difference between the two linear polarizations is about π. In order to meet the phase requirement under the incidence of RCP wave and LCP wave, 15 kinds of metal-particles cover the 2π phase in steps of 22.5° as shown in Fig. 2(c). The corresponding amplitudes are shown in Fig. 2(d). The 15 kinds of metal-particles rotate with different values of angle α to form 64 kinds of metasurface arrays as displayed in Fig. 3.

3. Calculation and analysis of performance

3.1. Focused and vortex beam manipulation

The proposed metasurface phase distribution satisfies the following relation:

$$\begin{cases} \varphi_{\mathrm{L}} = \dfrac{360^\circ}{\lambda}\left(\sqrt{x^2 + y^2 + f^2} - f\right), \\ \varphi_{\mathrm{R}} = l \cdot \arctan\left(\dfrac{y}{x}\right), \end{cases} \tag{5}$$

where φ_{L} and φ_{R} are the required phase distributions to generate focused and vortex beams under the incidence of LCP wave and RCP wave, and λ, f, and l represent operating wavelength, focal length, and topological charge, respectively. Figures 4(a) and 4(b) show the phase distribution of generated focused beam and vortex beam under the incidence of LCP wave and RCP wave, respectively. Figure 4(c) demonstrates the function schematic diagram of the switchable focused/vortex beam function.

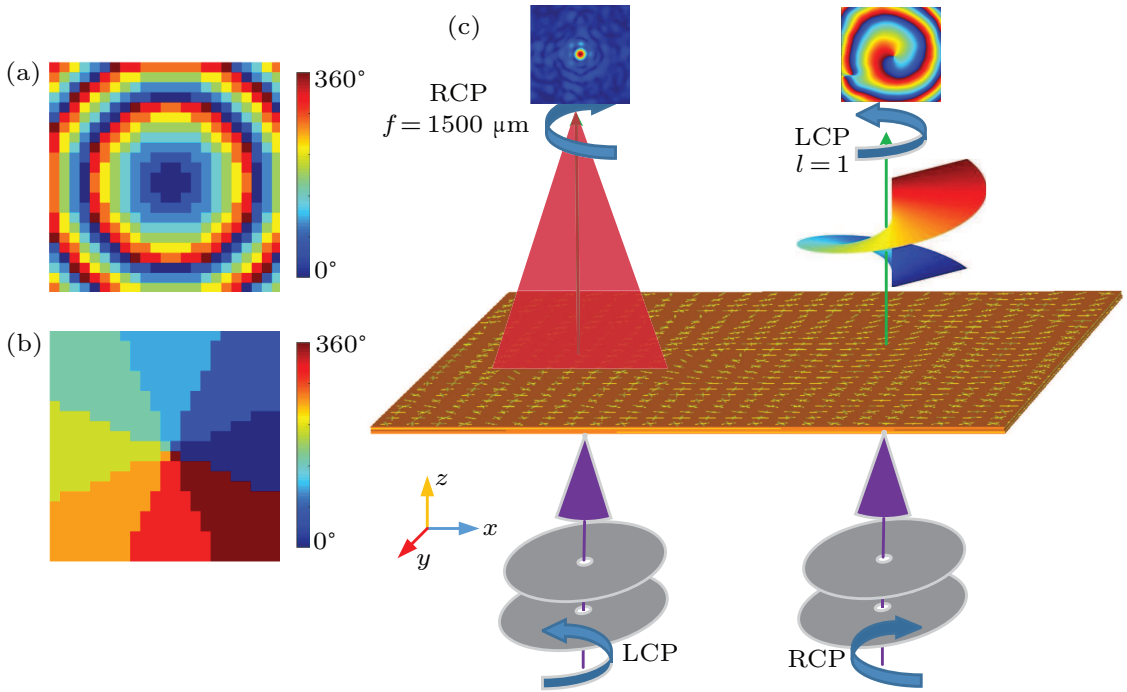


Fig. 4. (a) Focusing phase distribution under incidence of LCP wave, (b) vortex beam phase distribution under incidence of RCP wave, (c) function schematic diagram of switchable focused/vortex beam under incidence of LCP wave and RCP wave.

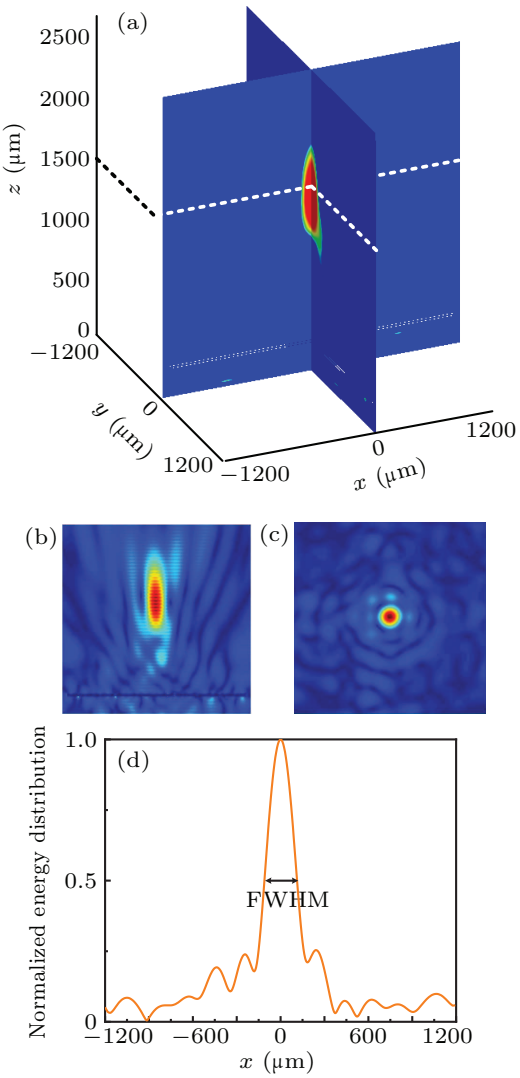


Fig. 5. Focusing effect under incidence of LCP wave: (a) energy distribution on *xoz* and *yoz* planes, (b)–(c) focal spot electric field strength in *xoz* and *xoy* planes, respectively, and (d) full width at half maximum in *xoy* plane.

Figure 5 displays the focusing effect of the proposed metasurface under the incidence of LCP terahertz wave at a frequency of 0.97 THz. The designed metasurface generates a terahertz focused beam with a focal length of $f = 1500$ μm as shown in Fig. 5(a). Figures 5(b) and 5(c) show the electric field intensity in the *xoz* plane and *xoy* plane, respectively. The focused spot can be clearly observed, and the electric field energy is focused on the center point. Figure 5(d) gives the full width at half maximum (FWHM) in the *xoy* plane, 0.224 mm (*i.e.* 0.721λ). That is to say, the proposed metasurface can obtain high-quality terahertz focused beam under the LCP incidence. Figure 6 describes the vortex beam effect with topological charge $l = 1$ when the RCP terahertz wave is vertically incident on the metasurface. The transmitted electric field phase, amplitude, three-dimensional (3D) far field, and mode purity of the vortex beam are shown in Figs. 6(a)–6(d), respectively. It can be seen from the figure that the mode purity of the vortex beam is 65.3%. Combining Figs. 5 and 6, it can be seen that the metasurface produces the focusing beam function and the vortex beam function under the incidence of LCP wave and RCP wave, respectively.

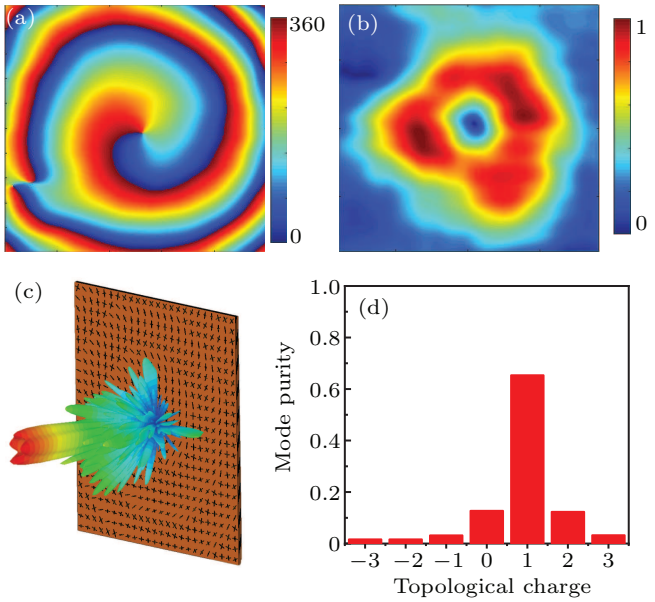


Fig. 6. Vortex effect under incidence of RCP wave: (a) phase distribution, (b) amplitude distribution, (c) 3D far-field, and (d) mode purity.

3.2. Vortex beam manipulation with different topological charges

The metasurface phase distribution satisfies the following relation:

$$\begin{cases} \varphi_{\mathrm{R}} = l_2 \cdot \arctan\left(\dfrac{y}{x}\right), \\ \varphi_{\mathrm{L}} = l_1 \cdot \arctan\left(\dfrac{y}{x}\right), \end{cases} \tag{6}$$

where l is the topological charge of the vortex beam, specifically, $l_1 = -1$ and $l_2 = -2$. The phase distributions of the vortex beams with different topological charges are shown in Figs. 7(a) and 7(b). Figure 7(c) shows the schematic diagram of vortex beams with different topological charges. Under the incidence of LCP wave, the proposed metasurface generates terahertz vortex beam with topological charge $l = -1$, and under the incidence of RCP wave, it generates vortex beam with topological charge $l = -2$. Figure 8 displays that the proposed metasurface generates a terahertz vortex beam with topological charge $l = -1$ under the incidence of LCP terahertz wave. At a frequency of 0.97 THz, the phase, amplitude, three-dimensional far-field, and mode purity of the generated vortex beam are shown in Figs. 8(a)–8(d). We can find that the mode purity is 68.7%. Figure 9 gives terahertz vortex beam with a topological charge number $l = -2$ under the illumination of the RCP wave. Figures 9(a)–9(d) represent the electric field phase distribution, amplitude distribution, 3D far field, and vortex beam mode purity of 55.4%, respectively. It can be noted from Figs. 8 and 9 that the designed metasurface can control vortex beam with different topological charge numbers under the incidence of LCP wave and RCP wave.

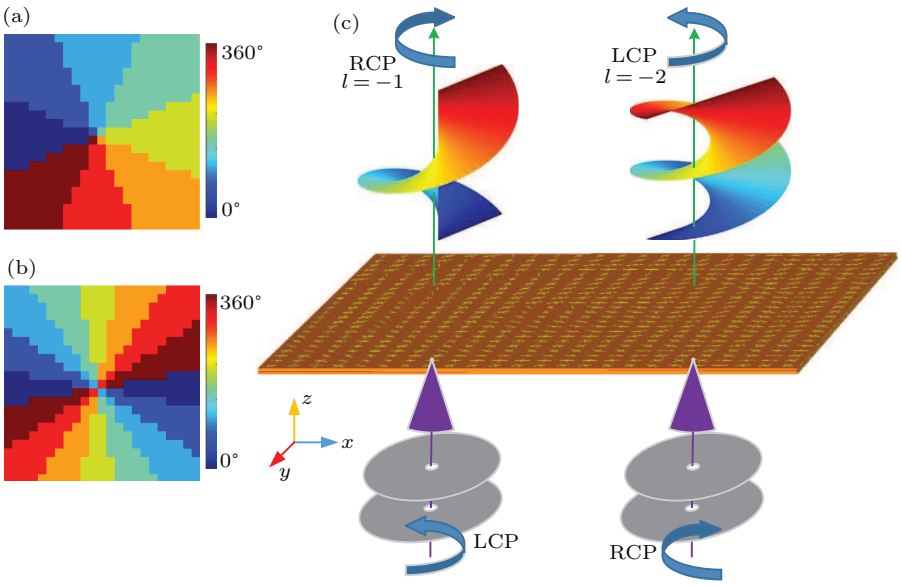


Fig. 7. (a) Vortex beam phase distribution with $l=-1$ under incidence of LCP wave, (b) vortex beam phase distribution with $l=-2$ under incidence of RCP wave, (c) vortex beam manipulation with different topological charges under incidence of LCP wave and RCP wave.

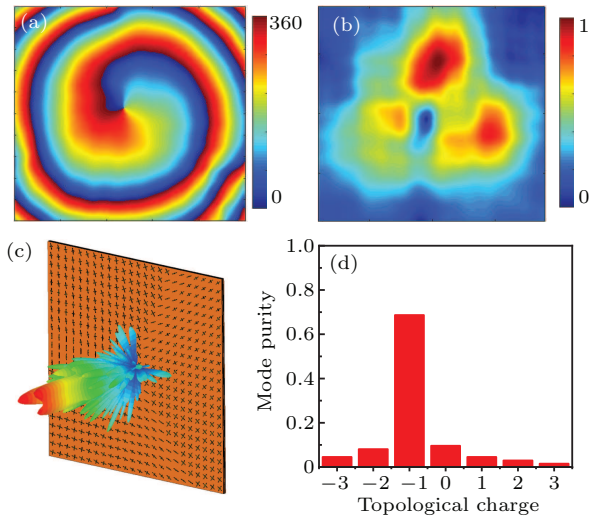


Fig. 8. (a) Phase distribution, (b) amplitude distribution, (c) 3D far-field, (d) mode purity for vortex beam with topological charge $l=-1$ under incidence of LCP wave.

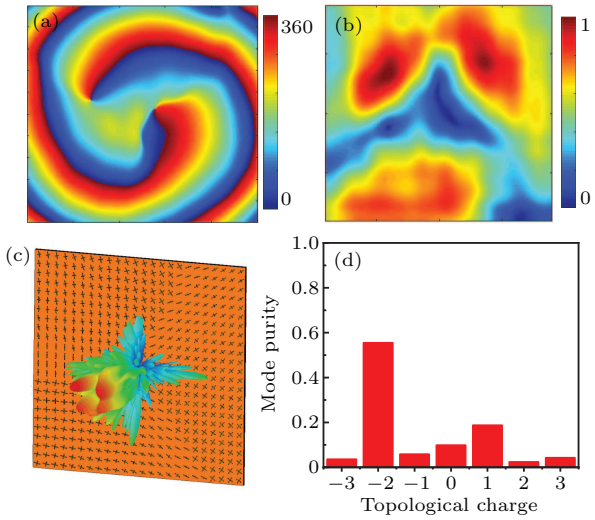


Fig. 9. (a) Phase distribution, (b) amplitude distribution, (c) 3D far-field, (d) mode purity for vortex beam with topological charge $l=-2$ under incidence of RCP wave.

3.3. Vortex beam direction manipulation

When the designed metasurface phase distribution satisfies the following formula:

$$\begin{cases} e^{i\varphi_R} = e^{i\varphi_{R1}} + e^{i\varphi_{R2}}, \\ e^{i\varphi_L} = e^{i\varphi_{L3}} + e^{i\varphi_{L4}}, \\ \varphi_{R1} = l_1 \cdot \arctan\left(\dfrac{y}{x}\right), \\ \varphi_{R2} = l_2 \cdot \arctan\left(\dfrac{y}{x}\right), \\ \varphi_{L3} = l_3 \cdot \arctan\left(\dfrac{y}{x}\right), \\ \varphi_{L4} = l_4 \cdot \arctan\left(\dfrac{y}{x}\right). \end{cases} \tag{7}$$

Here, l is the topological charge of the vortex beam, $l_1 = l_3 = 1$, $l_2 = l_4 = 2$. Figures 10(a) and 10(b) show the phase distribution of the proposed metasurface for generating vortex beams with different topological charges. Figure 10(c) shows that two vortex beams with different topological charges are generated along the x axis direction and the y axis direction under the incidence of LCP wave and RCP wave.

Figures 11(a) and 11(b) show the 3D far-field distribution and phase distribution of the terahertz vortex beam generated under the incidence of LCP wave at a frequency of 0.97 THz. It can be seen that the two terahertz vortex beams (marked as VB1 and VB2) with different topological charges ($l=1$ and $l=2$), in which the VB1 and VB2 are located in the $-x$-axis direction and the $-y$-axis direction, respectively. The VB2 aperture is slightly larger than the VB1 aperture, which is caused by the increase of the topological charge value. Under the incidence of the RCP wave, the 3D far-field distribution and the far-field phase distribution of the terahertz vortex

beams are given in the following Figs. 12(a) and 12(b), respectively. Two terahertz vortex beams with the $+x$-axis direction (named as VB3) and with $+y$-axis direction (named as VB4). It can be seen from the figure that the direction of the terahertz vortex beam can be effectively regulated under the incidence of the THz waves with different polarizations (*i.e.*, LCP/RCP). A comparison with other reported articles is shown in Table 1. According to Table 1 shown below, one can see that the designed metasurface has a relatively good performance and multi-function.

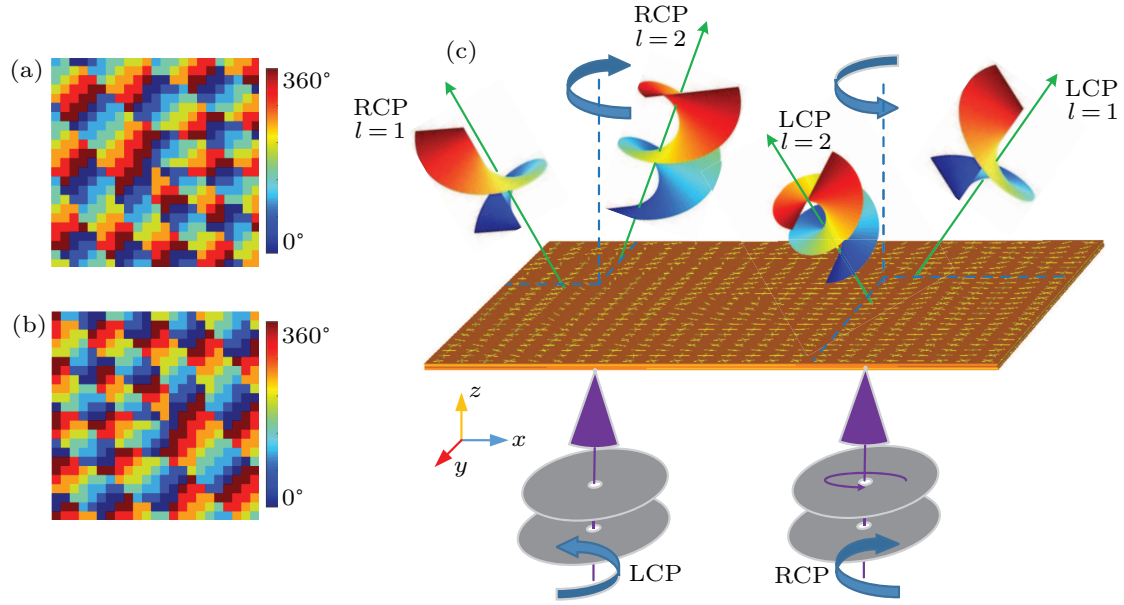


Fig. 10. Vortex beam phase distribution under (a) incidence of LCP wave, (b) RCP wave, and (c) function schematic diagram for directions switchable vortex beams with different topological charges under incidence of LCP wave and RCP wave.

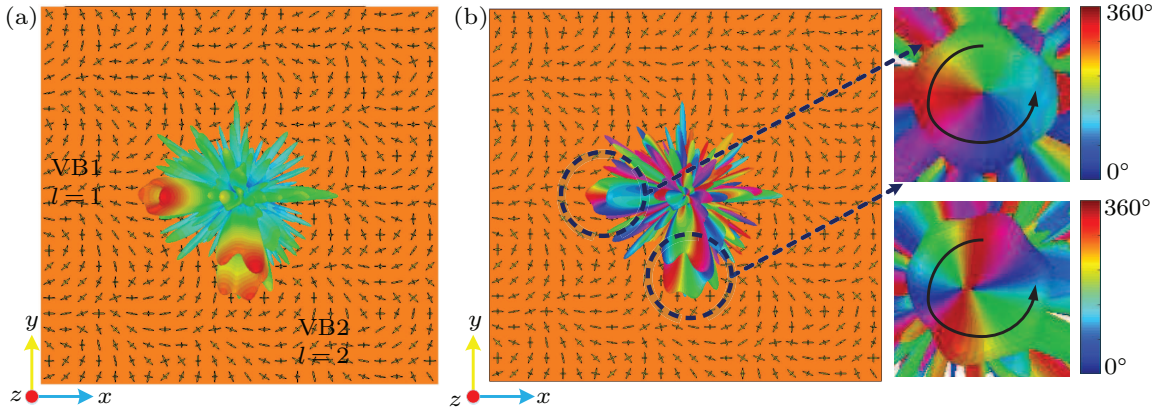


Fig. 11. (a) The 3D far-field and (b) phase distribution of generated vortex beam in $-x$ direction and $-y$ direction under incidence of LCP terahertz waves.

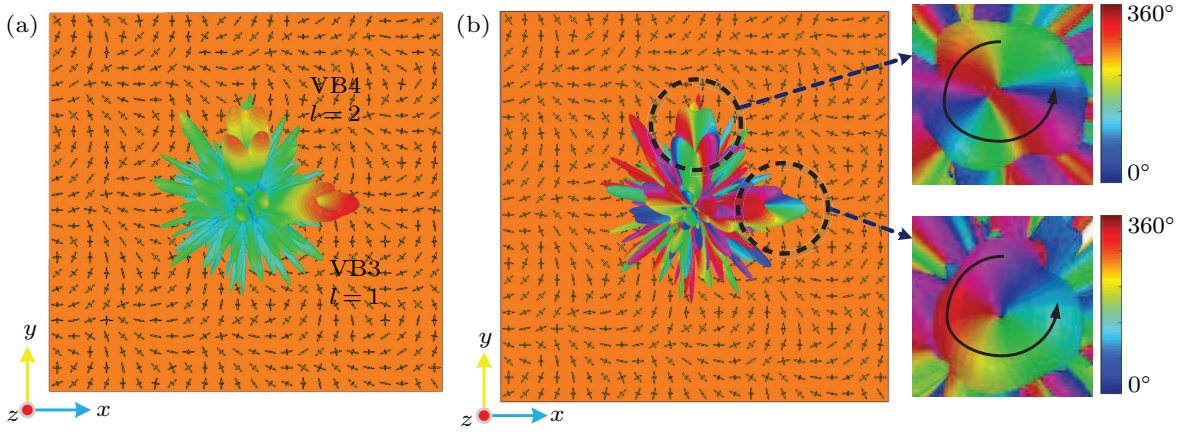


Fig. 12. (a) The 3D far-field and (b) phase distribution of generated vortex beam in $+x$-axis direction and $+y$-axis direction under incidence of RCP terahertz wave.

Table 1. Comparison of performance between proposed metasurface and some previous research results.

Ref.	Frequency (GHz)	Channel number	Mode of beams
[25]	9.5/15	2 (frequency)	1
[26]	8.7	2 (transmission & reflection)	1
This work	0.97	2 (LCP and RCP)	$-2/-1/1/2$

4. Conclusions

In this work, we proposed a diversified function metasurfaces under the incidence of LCP terahertz wave and RCP terahertz wave. The structure consists of three-layer elliptical metal crosses, four-layer dielectrics, and two-layer hollow metal circles, which are alternately superimposed. Under the incidence of LCP wave and RCP wave, the designed metasurface can independently control focusing beam and vortex beam, vortex beams with different topological charges, and two vortex beams with topological charges ($l = 1$, $l = 2$) located in different azimuths. The proposed metasurface can independently manipulate two orthogonal circularly polarized waves, which has great application values in the future multifunctional terahertz wave control devices.

Acknowledgements

Project supported by the National Natural Science Foundation of China (Grant Nos. 61871355, 61831012, and 62271460), the Talent Project of Zhejiang Provincial Department of Science and Technology, China (Grant No. 2018R52043), the Zhejiang Key Research and Development Project of China (Grant Nos. 2021C03153 and 2022C03166), and the Research Funds for the Provincial Universities of Zhejiang Province, China (Grant No. 2020YW20).

References

[1] Wang D, Li N N, Li Z S, Chen C, Lee B and Wang Q H 2022 *Opt. Express* **30** 3157
[2] Inoue K, Anand A and Cho M 2021 *Opt. Lett.* **46** 1470
[3] Lu H, Zheng B, Cai T, Qian C, Yang Y H, Wang Z J and Chen H S 2021 *Adv. Opt. Mater.* **9** 2001311
[4] Xu J W, Tian X M, Ding P, Xu K and Li Z Y 2021 *Opt. Express* **29** 44227
[5] Li X, Tang J and Baine J 2020 *Nanomaterials* **10** 1467
[6] Zhu W, Yang R S, Geng G Z, Fan Y C, Guo X Y, Li P, Fu Q H, Zhang F L, Gu C Z and Li J J 2020 *Nanophotonics* **9** 4327
[7] Liu J Q, Li X, Tao J Q, Dong D X, Liu Y W and Fu Y Y 2021 *Opt. Lett.* **46** 2537
[8] Zang X F, Yao B S, Li Z, Zhu Y, Xie J Y, Chen L, Balakin A V, Shkurinov A P, Zhu Y M and Zhuang S L 2020 *Nanophotonics* **9** 1501
[9] Jin R C, Tang L L, Li J Q, Wang J, Wang Q J, Liu Y M and Dong Z G 2020 *ACS Photon.* **7** 512
[10] Zhou L, Zhou T, Wang F, Li X, Chen R P, Zhou Y M and Zhou G Q 2021 *Opt. Laser Technol.* **143** 107334
[11] Hao W M, Wang J and Chen L 2021 *Opt. Lett.* **46** 4084
[12] Chen L, Liao D G, Guo X G, Zhao J Y, Zhu Y M and Zhuang S L 2019 *Front Inform. Tech. El* **20** 591
[13] Zhou L, Zhao G Z and Li X N 2019 *Acta Phys. Sin.* **68** 108701 (in Chinese)
[14] Zhang X D, Kong D P, Yuan Y, Mei S, Wang L L and Wang G X 2020 *Opt. Commun.* **465** 125561
[15] Sharma V, Aadhi A and Samanta G K 2019 *Opt. Express* **27** 18123
[16] Liu K Y, Wang G M, Li Z, Guo W L, Zhuang Y Q and Liu G 2019 *Opt. Commun.* **435** 311
[17] Jiang Q, Bao Y J, Li J, Tian L F, Cui T, Sun L, Du B W, Li B W, Bai B F, Wang J, Sun H B, Shen B, Zhang H, Lin F, Zhu X and Fang Z Y 2020 *Photon. Res.* **8** 986
[18] Zheng S, Hao H G, Tang Y H and Ran X H 2021 *Opt. Lett.* **46** 5790
[19] Liu Y T, Xie R S, Chen X, Zhang H L and Ding J 2021 *J. Phys. D: Appl. Phys.* **54** 475105
[20] Gao X and Tang L G 2021 *Acta Phys. Sin.* **70** 038101 (in Chinese)
[21] Ran Y Z, Liang J G, Cai T and Li H P 2018 *Opt. Commun.* **427** 101
[22] Gao X, Tang L G, Wu X B and Li S M 2021 *J. Phys. D: Appl. Phys.* **54** 075104
[23] Wang Y, Wang H, Su R F, Li S H, Tu X C, Wu J B, Zhang C H, Jin B B, Wang H B, Chen J and Wu P H 2021 *Opt. Express* **29** 33445
[24] Xiang Z Y, Shen Z and Shen Y C 2022 *Sci. Rep.* **12** 1053
[25] Iqbal, S, Madni H A, Liu S, Zhang L and Cui T J 2019 *Mater. Res. Express* **6** 125804
[26] Wu R Y, Zhang L, Bao L, Wu L W, Ma Q, Bai G D, Wu H T and Cui T J 2019 *Adv. Opt. Mater.* **7** 1801429